Ring Resonators: Materials, Technologies, Limits

Christoph Wächter

Fraunhofer Institute for Applied Optics and Precision Engineering
Albert-Einstein-Str.7, 07745 Jena, Germany

Abstract. There is a great potential of microring-resonators as optical add/drop-multiplex modules in photonics with very large scale integration. The area consumption per ring is incredibly small, and complex circuitry seems feasible. But, en route to application the production of ring resonators has to ensure specifications which can compete with those of other frequency periodic/selective devices. This ultimately leads to tight fabrication tolerances, and polarisation dependence and insertion loss of an unit enter the assessment as well. Capabilities to manufacture microring-resonator devices with different materials and technologies are valuated in this context.

INTRODUCTION

Within the last years there has been a very dynamic progress in the field of photonic applications for data- and telecom. Although much of the overdrawn expectations concerning the dynamics of data transport and telecommunication came down to earth, the number of optical components and devices which are mature for field application did escalate. This was based on improvements in technology and process engineering, and applies to both guided wave and free space optics.

A specific topic is the area-wide deployment of wavelength division multiplex (WDM), which dramatically improves the utilisation of the bandwidth provided by the optical fibre. The WDM-technology was applied in the long-haul lines primarily and spreads out to the metro and the access network, now. WDM basically requires wavelength selective filters, of course. Proven concepts like thin film interference filters (TFF) have been pushed to the limits with channel separations as low as 100 GHz corresponding to 0.8 nm in the 1.55 µm wavelength region, and new concepts from the guided wave optics field like the arrayed waveguide grating (AWG) have been developed to meet required specifications. The improvements in guided wave optics have been greatly assisted by the similarities of its technologies with those of microelectronics. And, just as in microelectronics, cost efficiency is related to the rate of yield and area consumption per device. In waveguide optics the guiding mechanism requires a rather big aspect ratio of lateral and longitudinal device dimensions. To reduce the absolute area consumption a high index contrast is necessary, which at the other hand facilitates the fabrication of devices like ring resonators with useful free spectral ranges for WDM applications.

To relate the potential of ring resonators in the WDM-field with other solutions, in a first section standard waveguide materials and related technologies are discussed. Next, WDM strategies and components are described, which define current standards of

CP709, *Microresonators as Building Blocks for VLSI Photonics: International School of Quantum Electronics, 39th Course,* edited by F. Michelotti, A. Driessen, and M. Bertolotti

specifications. Some basics of the physics of the ring resonator are recapitulated, and the requirements to meet those WDM-specifications with ring resonators are discussed in some detail. This finally leads to an evaluation of different waveguide materials and technologies with respect to their use for ring-resonator-devices.

MATERIALS AND TECHNOLOGIES FOR WAVEGUIDE OPTICS

Apart from hollow and anti-resonant reflecting optical waveguides (ARROW) conventional waveguides direct the light by total internal reflection. To this end, a laterally inhomogeneous refractive index distribution with an increased refractive index acting as the waveguide core has to be created. The cross section of the waveguide core is related to the index contrast and the index itself. $V = k_0 \sqrt{n_c^2 - n_0^2}\ d$ is the structural parameter of the slab waveguide with $k_0 = 2\pi / \lambda$ the free space wave-number, λ the vacuum wavelength, n_c the core and n_0 the base refractive indices respectively, and d the thickness. $V<\pi$ ensures monomode operation of the slab waveguide, and the corresponding thickness can be used as a first estimation of a edge length of a channel waveguide as a rule of thumb. For a 0.5% index contrast in a silica system in the C-band this comes to waveguide dimensions below 10 µm, where monomode silicon-on-insulator (SOI) waveguides require spatial dimensions below 0.5 µm, respectively. This, of course, necessitates more sophisticated patterning techniques.

What is related to the index contrast, too, is the minimum bending radius achievable, where the additional loss along an arc section or a curved waveguide, in general, stays below the losses due to its length. The losses of the straight waveguide are influenced by the material absorption, and by the sidewall roughness. Any sidewall roughness causes scattering, and the scattering rate is related to the index contrast, as well.

So, in general, different waveguide materials with related index differences result in quite different waveguide characteristics. Some of the most prominent including a number of typical technical specifications are indicated in table 1.

TABLE 1. Waveguide materials and related device characteristics,
(i) limited active material incorporation

Material	λ	Losses [dB/cm]	R_{min} [mm]	FC-Loss [dB]	Tuning	Wafer Size	Active	Process steps
polymers	VIS – (NIR)	0.1 … 2	20 ... 5	0.1 ... 0.5	T, E	... 12"	(i)	3 ... 20
ion exch.in glass	VIS-NIR	< 0.1	20	< 0.2	(T)	3"	(i)	< 10
silica on silicon	VIS-NIR	< 0.1	20 ... 2	0.1 … 2	(T)	4"	Er^+	~ 10
InGaAsP / InP	1.3 / 1.5µm	0.1 … 2	1 ... 0.05	1 ... 5	T,E,N	2"	inh.	10 .. >100
GaAlAs/ GaAs	0.8µm	0.5 … 2	1 ... 0.1	1 … 5	T,E,N	3"	inh.	10 ... 50
$LiNbO_3$	NIR	< 0.3	20	< 1	(T), A, N	4"	(i)	< 10

Polymers, e.g. acrylates, polyimides, polycarbonates and organically modified ceramics – ORMOCERs in short, [1,2] – can be utilized from the visible to the near infrared. Absorption in the NIR affects the relevant telecom wavelengths predominantly due to the O-H overtone, which can be greatly reduced e.g. by fluorinating the material. For 1.3 µm and 1.5 µm wavelength losses down to 0.1 dB/cm have been reached. Thermal stability often is termed to be critical and in fact depends on the particular material. Nowadays, optical polymers which withstand 250°C are available. Refractive indices of the polymers are in the range of 1.3 … 1.7. Minimum bending radii scale inversely with the index contrast and can go down to several millimetre. The fibre coupling (FC) loss to a standard telecom fibre can be held quite moderate. What is particular for polymers is the negative thermo-optical (TO) coefficient of ~ -10^{-4}/°K. Its magnitude makes polymer waveguides especially suited for thermo-optical tuning, indicated by the letter T in the tuning row of table 1. Electro-optical polymers are available as well, and there electrical tuning, E, is applicable, too. Wafer of almost any size can be used. Nonlinear materials, e.g. dyes, can be added to the monomere in the solvent to facilitate active devices. The number of basic process steps is very limited, especially when the patterning is accomplished by UV-exposure.

Ion exchanged waveguides profit by the low intrinsic loss of the glass and can have an index contrast very similar to that of the fibre. Thus, the FC-loss is very low, but, the bending radius is in the order of centimetres. Thermal tuning of glass waveguides is possible, in principle, but requires great temperature differences due to the low TO-coefficient. Wafer sizes do not exceed 3 inches. To incorporate active materials, they either have to be a constituent member of the glass matrix as in some chalcogenid glasses, or they have to be inserted via an ion exchange.

Silica on silicon, or glass on silicon, comprises techniques to produce glassy layers which consist of SiO_2, dominantly. Within flame hydrolysis deposition (FHD), one of the standard technologies, boron, phosphor, sulphur and germanium are added to tune its properties. In FHD, erbium can be added as well for amplifiers. For compact devices, the refractive index contrast can be pushed to several hundredths, which increases the FC-loss, if no special means like waveguide tapers are considered. The thermal tuning characteristics are poor, again. The wafer size is limited to 4 inches, typically, due to stability and reliability issues which go back to high processing temperatures in FHD and unequal coefficients of thermal expansion (CTE) of silicon and glass.

In semiconductors, either quaternary indium phosphide or ternary gallium arsenide, the base refractive index provokes a tighter confinement and higher FC-losses, consequently. Propagation losses are due to impurities and sidewall roughness, too. Electro-optical tuning capabilities are provided by the Franz-Keldysh-effect, the quantum-confined-Starck-effect or carrier injection and the plasma effect. Resonant and non-resonant $\chi^{(3)}$-effects are the basis for amplification, lasing, and sum- and difference frequency generation, indicated by a N in the corresponding row of table 1. The overall number of process steps can go to several hundred, if complex devices like distributed-feed-back lasers with integrated modulators are considered, where selective area growth facilitates to have a laser section with multiple quantum wells in a separate confinement heterostructure, and an absorption modulator on one and the same substrate.

Lithium-niobate is a crystalline waveguide material which is especially attractive for electro-optical modulation. Additionally, acoustic surface waves can be drawn on for signal processing. The photo-refractive effect and the absorption in the are VIS issues. For telecom wavelengths the waveguide loss is acceptable. The FC-loss is affected by the high refractive index itself and the fact, that Ti-diffusion or proton exchange, equivalently, produce surface waveguides. An appropriate second diffusion step can improve the matching of the waveguide and the fibre fields. The $\chi^{(2)}$-coefficient and periodical poling which causes domain inversion allow for second harmonic generation in lithium-niobate.

Obviously, there are much more materials which can be used for waveguide devices. Silicon-oxynitride, e.g., which is deposited by chemical vapour deposition (CVD), results in similar waveguides compared to FHD. What is of special interest is the possibility to increase the refractive index by an increase of nitrogen up to the limit of 2 for the pure silicon-nitride. To modify the material, germanium-hydrogen and phosphine can be added to the gaseous precursors. At the other hand, the N-H absorption band at 1.4 µm requires high temperature annealing in the SiON fabrication process. SOI is a material combination with a very high refractive index difference, which makes it well suited for photonic-crystal and ultra-compact waveguide devices. Diverse crystalline materials are known to be applicable as substrate, e.g. silicon on sapphire (SOS), or waveguide material directly, e.g. garnets or potassium-titanyl-phosphate. And, high index materials like Ta_2O_5 are used as pure films or in special glass compounds.

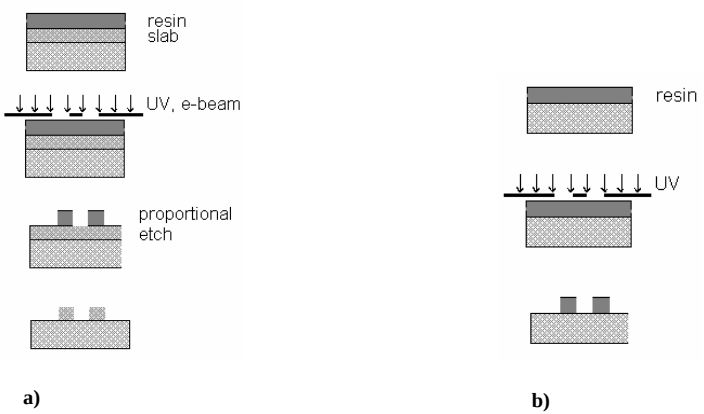

FIGURE 1. Basic steps of waveguide patterning. a) patterning of resin and subsequent proportional etch, b) direct patterning of waveguide material

The great majority of waveguide preparation techniques are planar ones, i.e. they start from the deposition of a layer or a sequence of layers, which act as a slab waveguide. This applies to e.g. benzocyclobutene, polycarbonate or acrylates to name a few of the polymers, and to glass on silicon, to SiON as well as to the semiconductor materials.

The layer deposition is simply a spin coating and a bake for polymers. In FHD the gaseous raw materials like $SiCl_4$ and $GeCl_4$ are converted to a soot of microparticles of

SiO_2 and GeO_2 by a oxyhydrogen combustion process, and the soot is consolidated to a glasslike material by a high temperature fusion. For the III-V materials the layer deposition is an epitaxial growth with a molecular beam epitaxy machine or metal-organic CVD.

After the layer deposition the slab is coated by a resin, which can be patterned either by e^--beam direct writing, or by UV-exposure of the whole wafer through a mask. Mask usage usually is much more efficient. If in the sub-micron region the feature size gets critical then the complex equipment of projection lithography may be required. At the other hand, e^--beam direct writing which is a standard for mask generation has a high resolution on its own. If the number of samples is limited and a high resolution is required, it can be the method of choice.

If the resin is patterned the structure is turned over to the guiding layer by a proportional transfer with an appropriate etch mechanism, e.g. reactive ion etching (RIE), an etch with an inductive coupled plasma (ICP), or a chemically assisted ion beam etching (CAIBE) process, see Fig. 1a for the routine.

A special point for the etch is the aspect ratio. If two waveguides are separated by a distance which is much narrower then the height of the guides, first any deviation from the vertical has an considerable impact, and, more serious, the hindered transportation of waste material in the slot or a hole may support a side-wall re-deposition which makes the precise adjustment of the gap width more difficult.

In general, the etch process introduces a side-wall roughness, too, which originates scattering. The loss rate is $\sim \Delta n^4 \, |r/\lambda|^2$, [3, 4], with r as the rms-value of the side-wall roughness and $\Delta n = n_c - n_0$ as the index contrast.

In the special case where the material of the guiding layer can be patterned directly, e.g. by an UV-induced polymerisation of a monomer with a photo-initiator added, any proportional transfer is needless. Here, in the developing step the unexposed material is removed by a washout, simply. Sidewall roughness is not an issue for the process sketched in Fig. 1b, but resolution is somewhat restricted compared to the patterning of a e^--beam resin. This is due to diffusion processes of free radicals, e.g., and nonlinear characteristics, which affect the exposure and the development, [5].

Another method to structure either the waveguide polymer directly or the resin for the proportional etch is a replication technology, [6]. What is needed first is a master which is to be prepared e.g. in silicon or quartz by lithography and etch steps as described above.

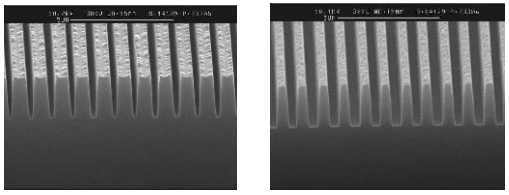

FIGURE 2. Replicas of gratings with $\Lambda = 1\mu m$ and different fill-factors in ORMOCER material

Then, from the master which is the inverse of the intended structure multiple 1:1 replicas can be generated e.g. by embossing. What is a critical step for this process is the

separation of the master and the replica, where mechanical forces have to be applied. Needle-like tips as they occur in waveguide branches tend to break off in an uncontrolled manner, which requires some precautions.

If the imprint technology is used for patterning the resin and a structure transfer via an etch step, a shallow master can be used which relieves the problems of the mechanical separation. The aspect ratio can be adjusted by the etch, afterwards. If inverse structures are prepared, a filling technique finally defines the waveguide core, [7].

Figure 2 exemplifies the potential of replication techniques with a grating structure of one micron period, and precise sub-micron features, accordingly, as an example.

Figure 3 sketches the waveguide preparation by ion exchange. In the case of $LiNbO_3$ Ti-stripes which are patterned lithographically define the waveguides. The Ti-in-diffusion increases the refractive index close to the surface. Another way to achieve this is a proton exchange, where Li-ions are replaced by hydrogen ions in benzoic acid. In a second step, a Mg-diffusion reduces the index at the surface, which as the result partially buries the index distribution.

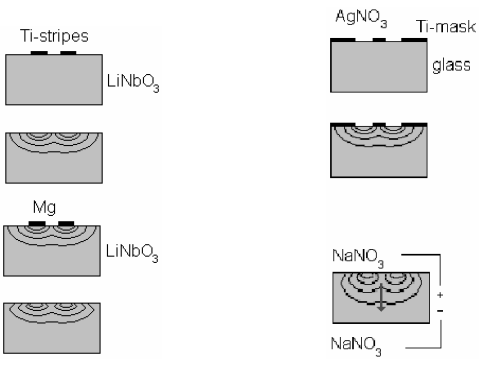

FIGURE 3. Waveguide preparation by ion exchange, a) in $LiNbO_3$, b) in glass

For the ion exchange in glass the openings of a Ti-layer define the path for the sodium-silver exchange. After the removal of the Ti, in a second field assisted exchange step, the index distribution is buried, and fibre matched mode profiles can be accomplished.

To resume so far, accuracy of waveguide patterning requires the precise adjustment of the layer parameter thickness and refractive index, first. Then, for the transfer of the mask structure, the intended width and any technology dependent suspension has to be taken into account as well as a depth profile, which may occur due to the etch or which is the result of the diffusion. The repeatability and the reliability of all process steps is mandatory if the process is to be transferred from the lab to the fab, and the device matures from the demonstrator status to the component which is ready for the market.

WDM STRATEGIES AND COMPONENTS

The use of multiple wavelengths requires multiplex and de-multiplex capabilities in order to facilitate the wavelength add and drop, or OADM in short (optical add/drop multiplex), at specific network nodes.

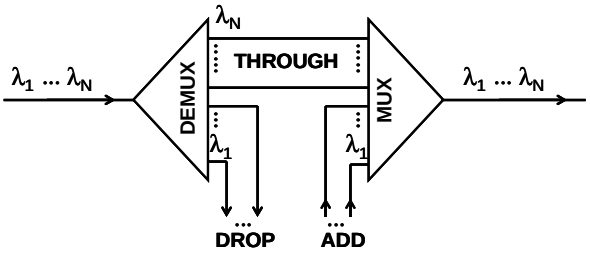

FIGURE 4. OADM based on DEMUX/MUX in parallel

The WDM-unit can rely either on a complete separation of all wavelengths at once, i.e. a treatment of all channels in parallel, or on a serial treatment of the wavelength channel by individual units, which is sketched in Figs. 4 and 5. The parallel WDM gives the best flexibility in channel use, simply due to the fact that all the individual wavelengths are manageable individually with just one unit.

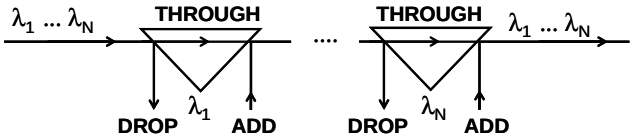

FIGURE 5. OADM based on serial DEMUX/MUX

This concept fits well if upgrades of the network capacity are envisaged. But, if a complete WDM is not intended the serial WDM with its low initial cost for the extraction of a single or a few wavelengths has its advantages. In contrast, a complete multiplex of a multitude of λ's serially would require a multitude of stages, and would multiply the loss.

Actual WDM-components which can be assigned to the different schemes above and which are applied in the network are AWG's for the parallel approach, and TFFs for the serial one. Fiber Bragg gratings (FBG) can address the serial WDM as well.

The sketch of an AWG is shown in Fig. 6. It's operation principle is based on the a successive length difference ΔL of the individual waveguides in the array,

$$L_i = L_0 + i\,\Delta L \tag{1}$$

Thus, the far field of the input waveguide(s) evolves within the first slab region, is transferred to the array waveguides with individual amplitudes, and experiences an individual phase shift in the array corresponding to the optical path length.

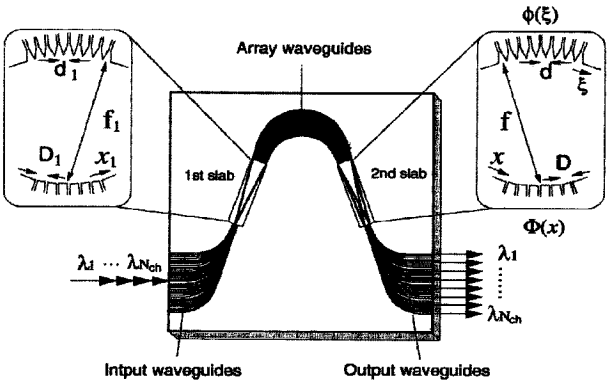

FIGURE 6. AWG-configuration, reprinted from [8]

The length difference is adjusted such that for the central wavelength of the AWG the optical path difference due to the length difference corresponds to a multiple of the wavelength in the individual channel waveguide,

$$n_{ch}\ \Delta L = m\lambda_0\,, \tag{2}$$

where n_{ch} is the effective index of the channel guided mode. At the entrance of the second slab the array waveguides form a grating with grating constant d. Constructive interference of the beams emerging from the array waveguides occurs corresponding to the grating equation

$$n_s\ d\sin(\Theta) + n_{ch}\ \Delta L = m\lambda\ , \tag{3}$$

i.e. the wavelength dependent optical path difference results in a change of the angle Θ, and a change of signal position in the focal plane, respectively. n_s is the effective propagation constant in the slab waveguide.

In other words, equations (2) and (3) characterise the AWG as a blazed grating (with blaze angle 0°) operated in order m. Thus, the AWG is inherently frequency periodic with a free spectral range (FSR):

$$FSR = \frac{\lambda_0}{m}\left(\frac{n_g}{n_{ch}}\right)^{-1}\ , \tag{4}$$

where n_g is the effective group index of the array waveguides. For a Gaussian amplitude distribution as input the envelope of the output signals vs. the wavelength is Gaussian as well. At the egde of the FSR 3 dB loss do occur, which reflects the power transfer into orders $m\pm1$. The individual output signal has a Gaussian amplitude distribution, and flat top options are manageable at the cost of some additional loss. The next neighbour cross-talk (CT) is mainly influenced by the receiver spacing, and phase errors in the array limit the cross-talk in general. What is apparent from equations (2-3) is the critical dependence of the AWG operation on the effective refractive indices. This indicates tight tolerances of the waveguide fabrication and the need for thermal stabilisation to suppress the influence of any TO-coefficient.

TABLE 2. Specifications for a standard AWG, 40 channels, 100 GHz channel spacing
IL (insertion loss), PDL (polarisation dependent loss), PMD (polarisation mode dispersion)

IL	IL unif.	PDL	PMD	CT	1 dB bandwidth	dλ/dT
5 dB	1 dB	0.4 dB	0.4 ps	-25 dB	0.25 dB	~0pm/°C @ 5 W

Table 2 shows some specifications of a standard 40 channel AWG with 0.8 nm channel spacing, operating in the C-band. Temperature influences are eliminated by fixing a temperature of about 70°C at the expense of 5W electrical power, approximately. Otherwise, an dλ/dT-value of 10 pm/°C, approximately, would emerge.

TFF's rely on the existence of a stop band in a periodic sequence of $\lambda/4$ layers of different refractive indices. Into this stop band, which is ~300 nm wide for a SiO_2 / TiO_2 layer system, a resonance is introduced by a $\lambda/2$ layer of appropriate thickness, Fig. 7. For a single cavity, the spectrum is too narrow at the center and too wide in the wings. With 3 to 7 cavities and up to 100 layers in total, flat-top filter curves can be achieved which fit to real telecom applications. What is to be considered is the fact, that the field of view (FOV) of the TFF, $\theta = 2\,\bar{n}\sqrt{(\Delta\lambda_{1/2})/\lambda_0}$ with $\bar{n}$ the averaged refractive index, is related to the band width $\Delta\lambda_{1/2}$, [9]. Thus, for a typical channel spacing in the range of a few 100 GHz, the angular spectrum of the modal field of the standard telecom fibre exceeds the TFFs FOV by far. This requires to operate the TFFs in a collimated beam.

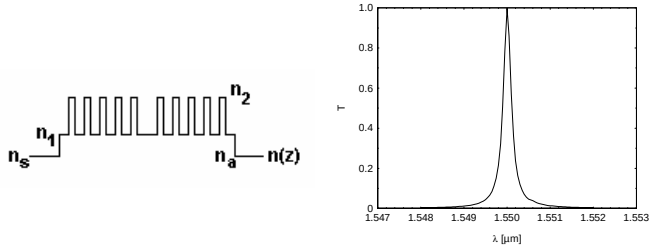

a) **b)**

FIGURE 7. Band pass interference layer system, a) layer structure, b) filter curve vs. λ

Typically, the beam transformation is done by round gradient index (GRIN) lenses of quarter pitch length, which transform the beam diameter from ~10 µm to several 100 µm. The non-central attachment of two fibres to one GRIN-lens results in a dual fibre collimator, from which a 3-port filter device can be derived without the additional need for an optical circulator, Fig. 8.

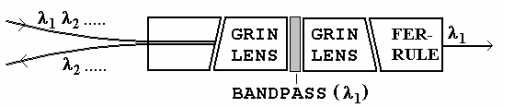

FIGURE 8. Sketch of a single stage TFF-element

Thus, TFFs for WDM-applications are typical micro-optical assemblies. What is of great importance is the fact, that with an appropriate substrate material the filter operates with negligible temperature dependence by an internal balance of TO-coefficient and CTE, [10]. Table 3 shows some specifications of a standard 16 channel TFF system with 100 GHz channel spacing.

TABLE 3. Specifications for a 16 channel, 100 GHz channel spacing TFF system

IL (mux)	IL (demux)	PDL	PMD	CT	1dB bandwidth	dλ/dT
7 dB	8 dB	0.15	0.1 ps	-25 dB	0.4 nm	0.5 pm/°C

What is to be noted is the IL of the single stage TFF which is about 0.5 dB in the through and about 1.5 dB in the add/drop ports, typically. Obviously, the internal structure of TFF-based multi-channel WDM-device has to be somewhat elaborated to come to a sufficient uniformity over the wavelength span. Beside the individual single stage TFF, shown in Fig. 8, interleaver filters, band separation filters, and attenuators are frequently used components.

Although TFFs are based on resonant cavities, a FSR does not play any role due to the fact that for low multiples of $\lambda/2$ for the cavity no other resonance frequencies are within the range of interest.

By comparison of AWG and TFF some of the individual advantages and disadvantages are evident. Obviously, AWGs have a higher degree of integration, and they allow for higher channel numbers than TFF-WDMs. At the other hand, the handling of a single channel is inappropriate for the AWG. The guided wave approach allows for an integration of additional functionalities at the wafer level. The micro-optical assembly, at the other hand, allows for a hybrid integration of nonreciprocal elements, too, which is out of the scope of the material systems for waveguide optics considered so far.

For other WDM techniques, potentially new ones, the specifications of tables 2 and 3 define a level, which has to be outperformed. Beside the technical specifications, another relevant aspect is an efficient use of area and/or volume. Compact devices with as

much monolithic integration as possible and with flexible channel count, preferentially, would fit to high yield production and cost efficiency.

RING RESONATOR BASICS

The simplest ring resonator configuration is a circular waveguide coupled to a straight one, Fig. 8a. This can be regarded as a directional coupler (DC) – with variable coupling distance – which is modified by a feedback mechanism through the ring.

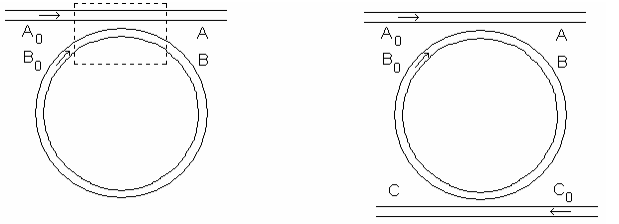

a) **b)**

FIGURE 9. Ring resonator configurations, coupling region indicated by dotted line

The directional coupler is described by the standard equations of coupled mode theory,

$$A = (1-\gamma)^{1/2}\left[A_0 \cos(\kappa l) - i\, B_0 \sin(\kappa l)\right] \tag{5a}$$

$$B = (1-\gamma)^{1/2}\left[-i\, A_0 \sin(\kappa l) + B_0 \cos(\kappa l)\right] \tag{5b}$$

with γ and κ as loss and coupling coefficients, and the product κl designates an effective coupling as an integral value along the DC. The mode evolution in the ring

$$B_0 = B\ \exp(-\sigma\pi\ R - i\Phi) \tag{6}$$

takes into account the loss per cycle, σ, and the phase of the mode, $\Phi = 2\pi\ R\beta$, with the propagation constant $\beta = k_0 \cdot n_{eff}$ and the ring radius R, respectively, [11]. With equations (5) and (6) the transmission is found as the ratio of A and A_0 :

$$T(\Phi) = \left|\frac{A}{A_0}\right|^2 = \left|(1-\gamma)^{1/2}\left[\frac{\cos(\kappa l) - (1-\gamma)^{1/2}\exp\left(-\frac{\rho}{2} - i\Phi\right)}{1 - (1-\gamma)^{1/2}\cos(\kappa l)\ \exp\left(-\frac{\rho}{2} - i\Phi\right)}\right]\right|^2 . \tag{7}$$

Complete slumps of the transmission occur when the numerator in equation (7) vanishes, i.e. when loss and coupling compensate, and if Φ is a multiple of 2π, too. This results in a periodic filter curve as it is shown in Fig. 10.

The phase condition gives the FSR, which simply reads as

$$\Delta\lambda_{FSR} = \frac{\lambda_0}{m} = \frac{\lambda_0^2}{n_{eff}\ 2\pi\ R} \tag{8}$$

when n_{eff} is assumed to be constant over the FSR for simplicity. Relevant characteristics of the ring resonator are the finesse F, which is the ratio of the FSR and the width of the individual resonance, $\delta\Phi$ or $\delta\lambda$, respectively,

$$F = \frac{2\pi}{\delta\Phi} = \frac{\Delta\lambda_{FSR}}{\delta\lambda} \tag{9}$$

and the Q-factor, which is a measure of the energy stored in the ring and the energy loss per cycle,

$$Q = 2\pi^2 \frac{n_{eff}}{\lambda_0} \frac{R}{\bar{\kappa}^2} \approx \frac{\lambda}{\delta\lambda} \tag{10}$$

where $\bar{\kappa}^2$ stands for the energy fraction coupled in the DC, and the group velocity in the ring waveguide is approximated by the phase velocity c/n_{eff}, [12].

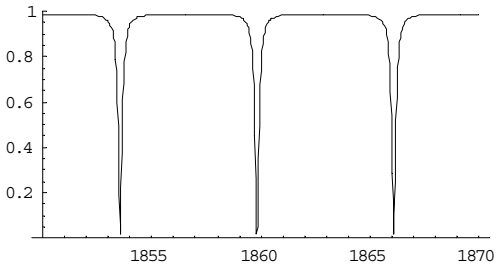

FIGURE 10. Transmission vs. Φ, 0.05 dB coupler loss, 0.5 dB ring loss, n_{eff}=1.46, and κl=0.3

From Fig. 10 it is evident, that ring resonators can be applied as wavelength selective filters, recalling the λ-dependence of Φ. By tuning the waveguide characteristics, frequency selective attenuators and modulators can be anticipated. 4-port configurations as depicted in Fig. 9b are candidates for serial OADM, and gain media would allow for laser devices. Potential implications may result from the wavelength dependency of the coupling coefficient, if broadband applications are considered. As for the single TFF-

cavity, the resonance of the single ring coupled to a bus waveguide is too narrow at the center and too wide in the wings. This problem can be removed the same way as for the TFF by cascading individual resonators, resulting in a flat top filter curve.

In essence, the ring resonator is a compact interferometer device. Thus, when its use is envisaged, a precise control of the resonance condition, and a precise control of coupling and loss are mandatory. Multi physics requirements occur for any intended tuning capabilities, as they are in the reach of thermo-, electro- or non-linear optics. What is to be noted explicitly is the fact, that the field enhancement in the ring is advantageous for non-linear processes like frequency mixing and switching, [13, 14].

RING RESONATORS AND WDM SPECIFICATIONS

For WDM applications specific criteria have to be met, e.g. channel allocation, channel separation, CT, IL, and a flat-top filter curve is mandatory as well. In an OADM device as sketched in Fig. 11, the latter is achieved by the ring cascade, situated in an upper and a lower waveguide plane.

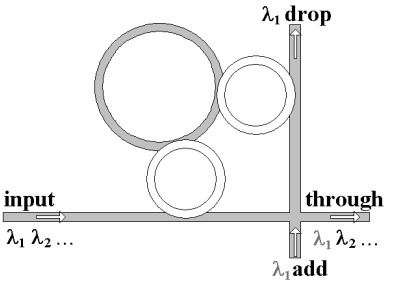

FIGURE 11. Top view of ring resonator based OADM device (dark waveguides in lower plane)

Looking at a standard WDM application with e.g. 16 channels a serial order of corresponding single channel devices would be required. For a spacing of 100 GHz in the C-band from equation (10) a lower limit of 1550 nm / 0.8 nm ~ 2000 for the Q-factor for the individual resonator can be read. The resonator processing the central wavelength would require a FSR of 13 nm, whereas 26 nm are required for the outer channels due to the symmetric position of the resonance within the FSR.

From equation (8) follows the relation of FSR intended and ring radius required, e.g. $R < 30 / n_{eff}[\mu m]$ for the 13 nm FSR. Inserting the Q-value in equation (10) the acceptable loss per cycle can be derived by recalling that the coupling $\overline{\kappa}^2$ compensates the ring loss, where the minor loss due to the DC is neglected for the moment. For the parameter from above, 0.5 dB/cycle would be the tolerable loss maximum in the ring.

As mentioned earlier, waveguide bends introduce losses. This can be understood from a simple explanation based on Fig. 12.

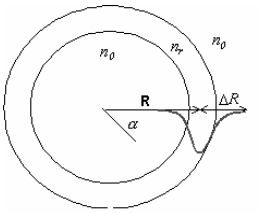

FIGURE 12. Ring waveguide

Looking at the centre of the waveguide at radius R, the phase velocity is

$$R\frac{d\alpha}{dt} = \frac{c}{n_{eff}} \ . \tag{11}$$

At some distance ΔR apart from the centre of the ring, the phase velocity reaches the speed of light in the substrate medium, i.e. any evanescent field out of $R+\Delta R$ with

$$\Delta R = \frac{n_{eff} - n_0}{n_o} R, \tag{12}$$

will be lost due to radiation. Thus, index contrast and ring radius are related, obviously. Recalling the fact, that the evanescent field outside the waveguide decays exponentially, a tolerance criterion can be set in order to limit the loss figure,

$$\exp\left(-k_0\sqrt{n_{eff}^2 - n_o^2}\,\Delta R\right) \le tol \tag{13}$$

The index contrast to meet this criterion follows from

$$\sqrt{\frac{(\Delta n)^3}{2n_0}} + \ln(tol)\cdot\frac{\lambda}{2\pi R} > 0 \tag{14}$$

where $n_{eff} \sim n_0+\Delta n/2$ has been assumed for simplicity. Although this model is far from being exact – which would require the excessive use of mode solvers for bend modes – it allows for a rapid estimation of the index contrast needed. Figure 13 shows the region, where the index contrast meets the requirements to facilitate an FSR of 13 nm for a *tol*-value of 0.1.

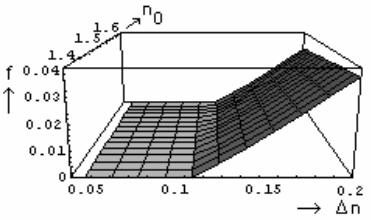

FIGURE 13. f>0 indicates applicable combinations of n and Δn for a FSR of 13nm

What has not been considered so far are losses due to the material itself and due to scattering, which has to be taken into account, too, for an exact analysis.

The accuracy of the optical path is the challenge which is to be accomplished. First, it is advisable to recall that the optical path in the ring corresponds to m waves in the medium, and one wave more or less covers a complete FSR. To position N channels within one FSR, the minimum accuracy thus is $\lambda_0/(n_{eff}\,N)$. To meet the resonance within the channel spacing with an accuracy of say at least 30%, for the 16 channel system the minimum accuracy needed is 1/50 waves, or 20 nm equivalently, for a hypothetic n_{eff}=1.5 at 1.5 µm wavelength. This clearly exceeds what is common for standard waveguide elements.

For a single channel filter, the usual $\lambda/10$ accuracy requirement for practical interferometric devices can be applied. For a ring radius of 15 µm, and n_{eff}=1.5 at λ=1.5 µm, this gives an relaxed relative accuracy of 10^{-3}, which applies to either the waveguide length or the effective mode index, equivalently. But, if the single channel device utilizes the maximum radius applicable for e.g. a 100 GHz wavelength separation, the relative accuracy goes down to 10^{-4}.

Due to the fact that the accuracy to be met is in waves, the requirements scale with the ring radius. Consequently, the combination of different low FSR rings to achieve a wider FSR by utilisation of the Vernier effect tightens up the accuracy demands.

To meet the coupling constants is an issue for ring to bus waveguide, as well as for ring to ring coupling. In [15] a fifth order interleaver filter has been investigated. What was found there and what is typical for higher order filters is the fact, that coupling efficiencies from a few % up to close to 100% can occur. The impact of a statistical variation of the coupling efficiencies by 10% of its nominal values was not critical for the throughput, but did deteriorate the rejection by 1/3 of its magnitude.

Due to the fact that the exponential field decay outside the waveguide directly enters the coupling constant,

$$\kappa \sim \exp\left(-k_0\sqrt{n_{eff}^{\,2}-n_0^{\,2}}\,g\right) \tag{15}$$

with g the gap between the relevant waveguides, the absolute accuracy which is to be met can be tiny. SOI configurations have gap distances in the order of 150 … 200 nm, typically, [16], which can be verified by simply calculating the supermodes of DCs.

Tolerable variations of the gap thus would be limited to 10 nm absolute, a value which is hard to be met.

With respect to the span of coupling efficiencies, another issue occurs. If a configuration of limited index contrast, e.g. n_0=1.6 and Δn = 0.2, is considered, cf. Fig. 13, the minimum length for almost complete power transfer for a DC with 1 µm x 1 µm waveguides and a straight coupling section comes down to approximately 15µm. This minimum coupling length occurs if the waveguides do just touch, simply due to the fact that there the difference of the effective propagation constants of the supermodes is maximum. The contact of the waveguides is unsuitable for several reason, and any finite gap increases the coupling length. If the FSR requires a very limited radius, thus, the maximum coupling efficiency achievable is limited due to an insufficient waveguide interaction. A working alternative to the lateral coupling thus is a vertical coupling, [17], which potentially results in a twofold benefit. First, the waveguides can be positioned one upon another, which gives additional degrees of freedom with respect to the adjustment of the coupling efficiency, and, the vertical gap does not need the etch of a tiny gap in the wafer plane. Instead, the thickness of a buffer layer is to be adjusted, which can relax the technological requirements.

In distinction, with a very high index contrast as in SOI, the minimum bend radius can be in the order of a couple of microns only, thus the optical path in the ring corresponding to the FSR can be deformed to a race-track geometry with an increased nominal gap value.

What is highly desirable for telecom applications is a polarisation independent device operation. This requires an identical propagation constant for both polarisations. For the individual waveguide without any residual birefringence in the materials thus a symmetric refractive index distribution and a quadratic core are advisable. But, the coupler geometry itself breaks the symmetry, and some asymmetry of the index distribution may occur due to the fabrication process. Thus, the accurate balance of both polarisation dependent coupling efficiency and propagation constant may require a precise tailoring of the waveguide cross section.

If those attempts fail, the alternative would be a polarisation splitting, the use of polarisation diverse devices, and a polarisation recombination. This, of course, is undesirable from the point of view of the total effort.

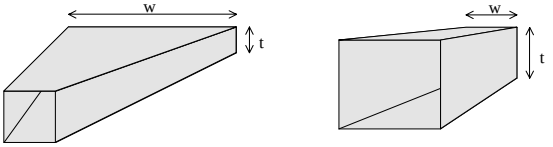

FIGURE 14. 3D-taper forms

The necessary index contrast for the ring resonator definitely leads to mode field diameter far below those of standard telecom fibers. Thus, butt coupling is inapplicable due to IL requirements. What is definitely needed is a spot size transformation, either by adiabatic tapers, Fig. 14, by the coupling between different waveguides, which needs

special coupling schemes, i.e. based on grating assisted directional couplers or n_{eff}-matched ARROWs, or by micro-optical approaches, e.g. lensed fibers.

To stay on the chip level, and to limit the number of different components needed at a chip, a taper technology, in 3D at the best, is advisable.

MATERIALS AND TECHNOLOGIES REVISITED

The list of requirements in order to realize ring resonator devices applicable in the WDM field with a FSR in the nanometer range is challenging, and effects a preselection of useful materials and technologies. First of all, the necessary index contrast rules out those waveguide technologies, which are focussed on low numerical aperture devices, produced by e.g. ion exchange in glass, by FHD and in $LiNbO_3$.

Other criteria are less stringent, and they enter the global assessment. For small footprint devices, the material loss is less critical. Effects of a residual birefringence in the waveguide material can be compensated by the design of the waveguide and a related technology in principle, [18, 19]. High temperature processes with SiON or SiO_2 layers on silicon substrates are prone to stress-induced birefringence due to different CTE. So, either CTE adaptation or low process temperatures a priori help to reduce this issue.

The thermal behaviour of ring resonator devices turns out to be a significant problem due to the TO-coefficient inherent to the individual materials. The requirement of a relative accuracy of 10^{-4} and less for the optical path, or $\lambda/50$ and less absolutely, self-evidently would squeeze the temperature range for proper operation. Thus, thermal stabilisation is unavoidable for any field use. The combination of glassy materials and a polymer cladding can reduce the temperature dependence of the filter characteristics due to the large negative TO-coefficient of the polymer, [20]. But, a complete elimination of the temperature dependence requires to adopt the confinement of the mode field, with detrimental side effects on polarisation and the accessible FSR.

At the other hand, fabrication tolerances can be compensated as well by trimming the refractive index by the required thermal stabilisation, or by UV-exposure, [21]. Thus, the fine-tuning of the resonance frequency for any individual device is feasible.

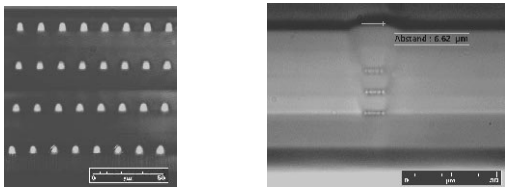

FIGURE 15. Vertically stacked waveguides in polymer (left) and SiON (right)

To take advantage of vertical coupling a technology with an excellent planarisation is mandatory. Spin coating of polymers can facilitate this, as it is apparent from Fig. 15. In SiON or similar materials, the surface profile of a lower waveguide layer reemerges as the surface profile of the subsequent buffer layer. This can be greatly reduced by a

special waveguide geometry as shown in Fig. 15, but this acts in opposition to polarisation independence, of course. Thus, either a high temperature reflow process or a chemical-mechanical polishing as in the semiconductor industry is necessary to flatten the buffer layer surface. Sub-micron thicknesses with tight tolerances for a buffer layer thickness can be achieved this way, and wafer bonding is another technique applicable for vertical coupling, [22].

The relative accuracy for the optical path is affected by the resolution of the lithography due to the mask writing process. Standard e^--beam writing equipment offers resolutions from 100 nm down to 25 nm, typically. Thus, with a precision of 25 nm for a 25 µm ring radius the device operation will fail for almost any WDM application. The resolution enters the wavguide width as well. Even for a 1.5 µm x 1.5 µm waveguide with index contrast of not more than Δn=0.2, a 25nm change of the waveguide width causes a $\Delta n_{eff} / n_{eff} > 10^{-4}$, which affects both multi-channel and low FSR operation as noticed above.

This situation can be improved by writing a continuous path, e.g. with the e^--beam machine LION LV-1 of Leica Microsystems Jena. Laser direct writing systems allow for continuous path as well, but there the minimum feature size may be problematic for narrow gaps, which in consequence would require a projection lithography additionally, to scale sizes down.

Another technology related fact is the influence of the side-wall roughness. It leads to scatter loss, first, and may excite backward propagating waves, too. Due to the inherent periodicity of the field, propagating many cycles in the ring, the influence of the reflection gains weight and may impact the filter curve, [4]. As mentioned above, the scattering rate is $\sim \Delta n^4$, thus high index contrast waveguides are more susceptible, and a weak coupling from bus to ring waveguides is more vulnerable, too.

If a ring resonator device concept for a passive WDM application is considered, and no constraints apply to the choice of material and technology, from the above some suggestions can be adopted:

- the index contrast should not exceed its lower limit too much,
- vertical coupling should be regarded for precise gap control and tight coupling, too,
- specifications for field-use have to be considered with respect to the trim range budgeted,
- limits for the mask resolution and roughness should be defined early in the design process to avoid mistrials,
- mode field adaptation to the telecom fibre should take place on chip via 3D waveguide tapers wherever applicable.

Clearly, the minimum bending radii limit the FSR, and, even for the maximum index contrast in SOI with e.g. a 5 micron ring diameter, coarse WDM is out of the reach. But, in dense WDM with channel spacings of 100 GHz and below, ring resonators show its special advantages, where compactness is the most prominent one. In principle, due to the low area consumption per ring, the serial WDM can be advantageously applied even if a complete wavelength separation of a multitude of narrow spaced channels is intended.

If semiconductor devices are considered, losses in the ring resonator can be compensated by amplifiers, and a wide range of capabilities for trimming, modulation and switching is accessible, additionally.

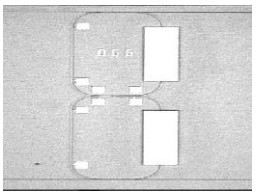

FIGURE 16. Ring resonator add / drop device in InP with integrated SOAs (large white areas) and Pt-resistors (contact pads – small white areas), photograph by courtesy of FhG-HHI

Figure 16 presents a notable example for an active ring resonator device which has been realised recently in InP. It consists of two rings with integrated semiconductor optical amplifiers and trim electrodes, [23]. The filter curve has the improved shape compared to the Lorentzian curve of the single ring filter as it is anticipated from the design.

In passive materials, remarkable progress has been achieved as well. In particular, within a specific glass material, deposited by a CVD process, multi-ring resonator filters with up to 6 coupled rings were successfully fabricated, [24-26]. What needs special attention is the fact that devices with low insertion loss, polarisation independence and flat top filter curves could be realized.

SUMMARY

Ring resonators are devices which are well suited for serial WDM and related applications, in principle. They allow for complex filter characteristics by a serial and / or parallel concatenation of individual rings. Due to the fact, that ring resonators in WDM applications in the telecom field require low bending radii per se, they result in compact devices and facilitate a high integration density.

This, at the other hand, requires challenging fabrication tolerances with respect to the waveguide preparation, and trim options for the compensation of manufacturing tolerances and temperature influences are unavoidable.

Within the last decade, outstanding technical progress has been achieved, which now allows for first practicable devices. So, ring resonators seem to be en route from their enfant stage to the competition with existing WDM solutions.

ACKNOWLEDGEMENT

The author would like to thank Helmut Heidrich from the Heinrich-Hertz-Institute, Berlin, for helpful discussions and for the photograph of the ring resonator device with integrated SOA, Fig. 16.

REFERENCES

1. H. Wolter, W. Glaubitt, and K. Rose, Mat. Res. Soc. Symp. Proc., **271**, 719-724 (1992)
2. R. Houbertz, et al., Thin Solid Films **442,** 194–200 (2003)
3. W. Karthe, and R. Müller, *Integrierte Optik*, Akad. Verlagsgesellschaft Geest & Portig, Leipzig, 1991, pp. 29-30
4. B.E. Little and J.-P. Laine, Optics Letters, **22**, 4-6 (1997)
5. U. Streppel, et al., Applied Optics, **42**, 3570-3579 (2003)
6. M.T. Gale, R.E.Kunz, and H.P.Zappe, Optical Engineering, **34**, 2396-2406 (1995)
7. C. Chao, and L.J. Guo, J.Vac.Sci.Technol., B**20**(6), 2862-2866 (2002)
8. Reprinted from K. Okamoto, *Fundamentals of Optical Waveguides*, Academic Press, San Diego, p. 347, Copyright (2000), with permission from Elsevier
9. P. Yeh, *Optical Waves in Layered Media*, Wiley, New York, 1988, pp. 162
10. H.Takashashi, Applied Optics, **34**, 667-675 (1995)
11. K. Okamoto, *Fundamentals of Optical Waveguides*, Academic Press, San Diego, 2000, pp. 161-163
12. B.E. Little, et al., Journal of Lightwave Technol., **15**, 998-1005 (1997)
13. V. Van, et al., IEEE Photonics Technology Letters, **14** , 74-76 (2002)
14. J.E. Heebner, R.W. Boyd, and Q-H. Park, JOSA B, **19**, 722-731 (2002)
15. A. Melloni, and M. Martinelli, Journal of Lightwave Technol., **20**, 296-303 (2002)
16. A. Vörckel, et al., IEEE Photonics Technol. Lett., **15**, 921-923 (2003)
17. B.E. Little, et al., IEEE Photonics Technol. Lett., **11**, 215-217 (1999)
18. A. Kilian et al., Journal of Lightwave Technology, **18**, 193-198 (2000)
19. G.-L. Bona, R. Germann, and B. J. Offrein, IBM Journal Res. & Dev., **47**, 239-249 (2003)
20. S.T. Chu, et al., IEEE Photonics Technol. Lett., **11**, 1138-1140 (1999)
21. S.T. Chu, et al., IEEE Photonics Technol. Lett., **11**, 688-690 (1999)
22. D.V. Tishinin, et al., IEEE Photonics Technol. Lett., **11**, 1003-1005 (1999)
23. D.G. Rabus, et al., IEEE Journal Selected Topics Quant. Electr., 8, 1405-1411 (2002)
24. B.E. Little, and S.T. Chu, Optics and Photonic News, **11**, 24-29 (2000)
25. http://www.littleoptics.com/OFC.pdf (B.E. Little, OFC 2003)
26. http://www.littleoptics.com/hofilter.pdf (press release Little Optics, 10/09/03)